






Article

New Pyrazole-Hydrazone Derivatives: X-ray Analysis, Molecular Structure Investigation via Density Functional Theory (DFT) and Their High In-Situ Catecholase Activity

Khalid Karrouchi ^{1,2,3}, El Bekkaye Yousfi ⁴, Nada Kheira Sebbar ⁵, Youssef Ramli ¹, Jamal Taoufik ¹, Younes Ouzidan ⁶, M'hammed Ansar ¹, Yahia N. Mabkhot ^{7,*} , Hazem A. Ghabbour ⁸  and Smaail Radi ^{2,*} 

¹ Laboratoire de Chimie Thérapeutique, Faculté de Médecine et de Pharmacie, Université Mohammed V, P. O. Box 8007, Rabat 10100, Morocco; khalid.karrouchi@um5s.net.ma (K.K.); yramli76@yahoo.fr (Y.R.); jataoufik@hotmail.com (J.T.); ansarmhammed@gmail.com (M.A.)

² Laboratoire de Chimie Appliquée et Environnement (LCAE), Faculté des Sciences, Université Mohamed I, P. O. Box 524, Oujda 60000, Morocco

³ Laboratoire National de Contrôle des Médicaments, Direction du Médicament et de la Pharmacie, Ministère de la Santé, P. O. Box 6206, Rabat 10100, Morocco

⁴ Institution Supérieure des Professions Infirmières et Techniques de Santé, P. O. Box 4806, Oujda 60000, Morocco; yousfi@netcourrier.com

⁵ Laboratoire de Chimie Organique Hétérocyclique, Pharmacochimie, Faculté des sciences, Université Mohammed V, P. O. Box 8007, Rabat 10100, Morocco; snounousebbar@gmail.com

⁶ Laboratoire de Chimie Organique Appliquée, Faculté des Sciences et Techniques, Université Sidi Mohamed Ben Abdellah, P. O. Box 2202, Fès 30000, Morocco; younes.ouzidan@usmba.ac.ma

⁷ Department of Chemistry, Faculty of Science, King Saud University, P.O. Box 2455, Riyadh 11451, Saudi Arabia

⁸ Department of Pharmaceutical Chemistry, College of Pharmacy, King Saud University, P. O. Box 2457, Riyadh 11451, Saudi Arabia; ghabbourh@yahoo.com

* Correspondence: yahia@ksu.edu.sa (Y.N.M.); s.radi@ump.ac.ma (S.R.); Tel.: +212-536-500-601 (S.R.)

Received: 18 September 2017; Accepted: 21 October 2017; Published: 25 October 2017

Abstract: The development of low-cost catalytic systems that mimic the activity of tyrosinase enzymes (Catechol oxidase) is of great promise for future biochemistry technologic demands. Herein, we report the synthesis of new biomolecules systems based on hydrazone derivatives containing a pyrazole moiety (**L1–L6**) with superior catecholase activity. Crystal structures of **L1** and **L2** biomolecules were determined by X-ray single crystal diffraction (XRD). Optimized geometrical parameters were calculated by density functional theory (DFT) at B3LYP/6–31G (d, p) level and were found to be in good agreement with single crystal XRD data. Copper (II) complexes of the compounds (**L1–L6**), generated in-situ, were investigated for their catalytic activities towards the oxidation reaction of catechol to *ortho*-quinone with the atmospheric dioxygen, in an attempt to model the activity of the copper containing enzyme tyrosinase. The studies showed that the activities depend on four parameters: the nature of the ligand, the nature of counter anion, the nature of solvent and the concentration of ligand. The Cu(II)-ligands, given here, present the highest catalytic activity ($72.920 \mu\text{mol}\cdot\text{L}^{-1}\cdot\text{min}^{-1}$) among the catalysts recently reported in the existing literature.

Keywords: pyrazole; hydrazone; crystal structure; DFT; catecholase activity

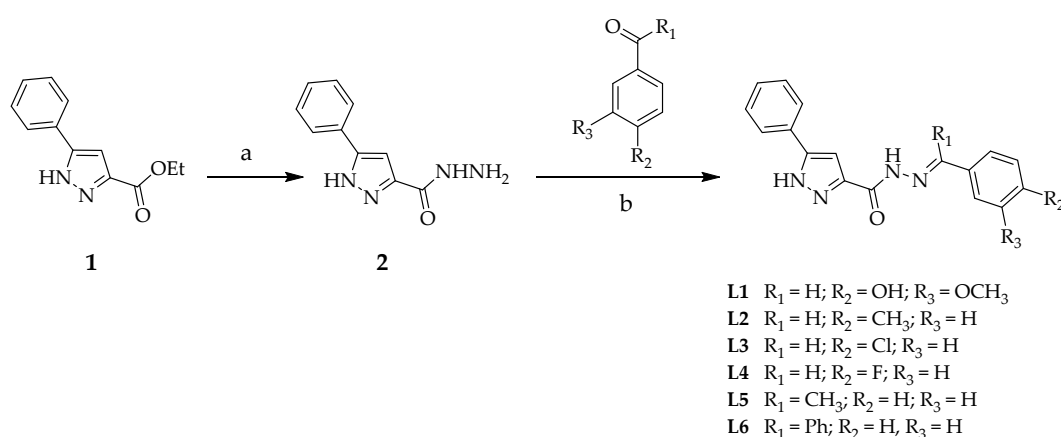
1. Introduction

Bioorganometallic compounds are reputed for their remarkable applications in the field of catalysis; however, much less is known about their potential in chemical biology [1,2]. An important goal in organometallic chemistry is the synthesis of biomolecules that exhibit catalytic activity analogous to the activity of enzymes. A number of catalysts having biomimetic activity for different enzymes have been designed by chemists [3,4]. The preparation and etude of efficient template complexes for metalloenzymes with oxidase or oxygenase activity are thus most important for the elaboration of new veritable catalysts for oxidation reactions [5]. Copper ions, as centers of potent site of various metalloproteins, play an essential role in several biological processes: electron transfer, oxidation, transport of dioxygen, etc. [6,7]. Copper complexes of low molecular weight are studied as structural and functional models of active centers of enzymes with copper [8–11].

Catechol oxidases perform the oxidation of 1,2-diphenols, such as catechol, to *o*-quinones, using dioxygen (O₂). Hydrogen atoms removed from catechol combine with oxygen to form water. The crystal structures of different forms of catechol oxidase have improved the accordance of the mechanism of catecholase activity of catechol oxidase. Several workers proposed the mechanism of catechol oxidation by natural enzyme, including important proposals by Solomon and kerbs [12,13]. In addition to the high number of Cu(II) complexes reported, their catecholase activity has also been demonstrated, although their mechanistic aspects are not as well understood as those of Cu(II) complexes [14–18].

Hydrazones are members of the Schiff bases family, which are built with aromatic acid hydrazides and carbonyl compounds. They are quite interesting in coordination chemistry as they present a combination of donor sites, such as a protonated/deprotonated amide oxygen atom, imine nitrogen atom of the hydrazone moiety and an additional donor site (usually N or O) provided from the aldehyde or ketone [19,20]. Hydrazones form wide variety of complexes with chemical, structural, biological and industrial importance [21–23]. These proprieties are attributed to the formation of stable chelate complexes with transition metals which catalyze physiological processes [24,25].

In this study, we report the synthesis of six new hydrazone derivatives containing pyrazole moiety with a good yield (Scheme 1). The X-ray crystal structures of compounds **L1** and **L2** were determined, and their geometrical parameters were compared with theoretical DFT calculations at the B3LYP level of theory. The investigation of catalytic activities of copper (II)-ligand complexes towards oxidation of catechol to *o*-quinone was studied. All of the parameters that can affect the catalytic efficiency were studied.



Scheme 1. The synthetic routes of compounds **L1–L6**: (a) hydrazine hydrate (80%), ethanol, reflux 5h; and (b) ethanol, acetic acid, reflux, 2–5 h.

2. Results

2.1. Synthesis

Synthesis of hydrazones (**L1–L6**) is outlined in Scheme 1. Starting compound, ethyl 3-phenyl-1*H*-pyrazole-5-carboxylate (**1**), was readily synthesized by the reaction of ethyl-2,4-dioxo-4-phenyl-butanoate, obtained from acetophenone, and diethyl oxalate, with hydrazine in the presence of sulfuric acid at room temperature. The reaction of ethyl 3-phenyl-1*H*-pyrazole-5-carboxylate (**1**) with hydrazine hydrate in ethanol afforded 3-phenyl-1*H*-pyrazole-5-carbohydrazide (**2**). Finally, the novel desired hydrazones (**L1–L6**) were obtained by condensing compound (**2**) with aromatic aldehydes at reflux of ethanol using acetic acid as reported in our previous procedure [26–28]. The expected products were isolated as crystalline materials with reliable to excellent yields.

2.2. X-Ray Crystal Structures Description

Compounds **L1** and **L2** were analyzed by X-ray diffraction. Refinement parameters and crystal data are listed in Table S1. Supplementary data are deposited with the Cambridge Crystallographic Data Centre (CCDC) under deposition numbers 1522882 and 1523265.

The selected bond lengths and bond angles and hydrogen bonds are listed in Tables S2–S5 in the Supplementary Materials. The asymmetric unit of **L1** contains one independent molecule with DMF and water molecules as mixed crystallizing solvent, as shown in Figure 1. All the bond lengths and angles are in normal ranges. In the crystal wrap, molecules are connected via many classical and non-classical intermolecular hydrogen bonds (Table S3). Figure 2 shows the crystal structure of **L2**. In the crystal structure, the pyrazole ring (N1/N2/C7–C9) makes dihedral angles with the phenyl ring (C1–C6) and tolyl ring (C12–C17), at 23.39° and 36.16°, respectively. In the crystal wrap, molecules are linked via two classical intermolecular hydrogen bonds between N1—H1N1...O1i and N3—H1N3...N2ii, Symmetry codes: (i) $x, -y+1, z+1/2$; and (ii) $-x+1, y, -z+3/2$ (Table S5).

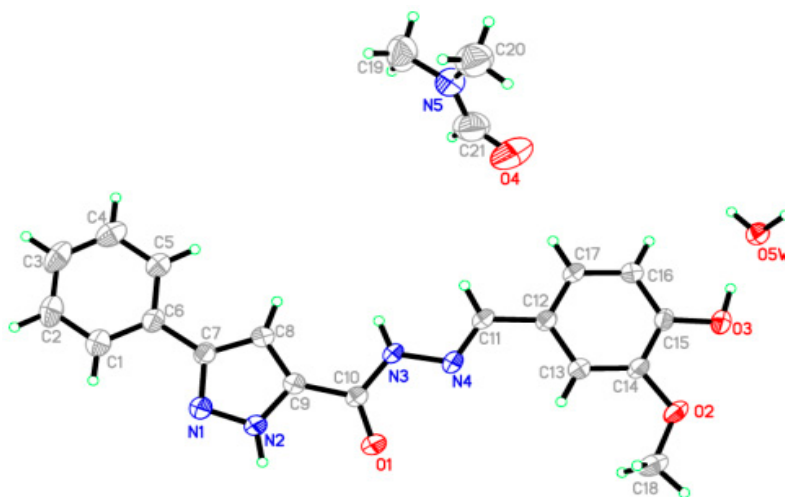


Figure 1. Asymmetric unit of **L1** (CCDC 1522882).

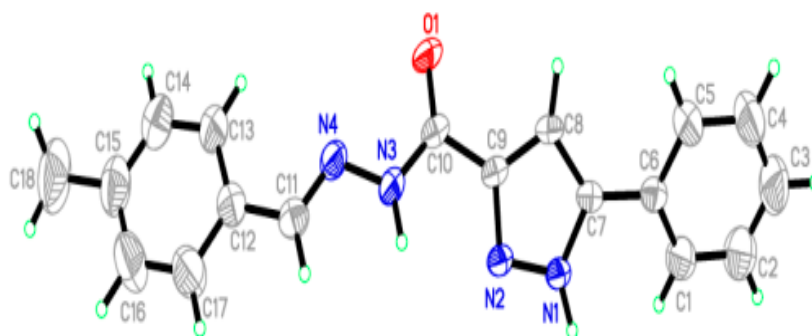


Figure 2. Asymmetric unit of **L2** (CCDC 1523265).

2.3. Computational Studies

Comparison of the theoretical values with the experimental ones indicates that all the optimized bond lengths are closer to the experimental values. In the case of X-ray structure of compound **L1**, the observed bond lengths of C1–C10, O3–C15 and N3–N4 bonds in five-membered pyrazole ring are 1.227(3) Å, 1.363(3) Å and 1.383(3) Å, respectively. The calculated bond lengths, through DFT method, of same pyrazole ring are 1.24394 Å, 1.38125 Å and 1.37144 Å, respectively, which are very close to the actual values. In Table 1, it is clear that actual C–C and C–H bond lengths are also in close agreement with calculated values. The calculated bond angles for O1–C10–C9, C14–O2–C18 and N4–C11–C12 bond angles of **L1** are 122.22°, 118.52°, 121.37°, respectively, which are close to the corresponding actual angles obtained from X-ray. The actual values of above bond angles are 121.3°, 118.3°, and 122.9°, respectively.

Table 1. Selected structural parameters by X-ray and theoretical calculations of compound **L1**.

Bond Length (Å)	Experimental Bond Lengths	Calculated Bond Lengths	Bond Angle (°)	Experimental Bond Angles	Calculated Bond Angles
O1–C10	1.22(3)	1.24	N2–C9–C8	106.0(2)	109.2
O2–C14	1.36(3)	1.39	O1–C10–N3	122.8(2)	125.0
O2–C18	1.41(4)	1.45	N3–C10–C9	116.0(2)	112.7
O3–C15	1.36(3)	1.38	O1–C10–C9	121.3(2)	122.2
N1–N2	1.33(3)	1.37	N4–C11–C12	122.9(2)	121.3
N1–C7	1.33(3)	1.38	O2–C14–C13	125.7(2)	126.0
N2–C9	1.34(3)	1.36	C14–O2–C18	118.3(2)	118.5
N3–N4	1.38(3)	1.37	N2–N1–C7	105.3(2)	113.2
N3–C10	1.34(3)	1.38	N1–N2–C9	112.6(2)	105.0
N4–C11	1.27(3)	1.29	N4–N3–C10	119.5(2)	121.0

The optimized geometry of compounds **L1** and **L2** were obtained at B3LYP/6-31G* level. Some optimized geometric parameters are also listed in Figure 3, and Tables 2 and 3.

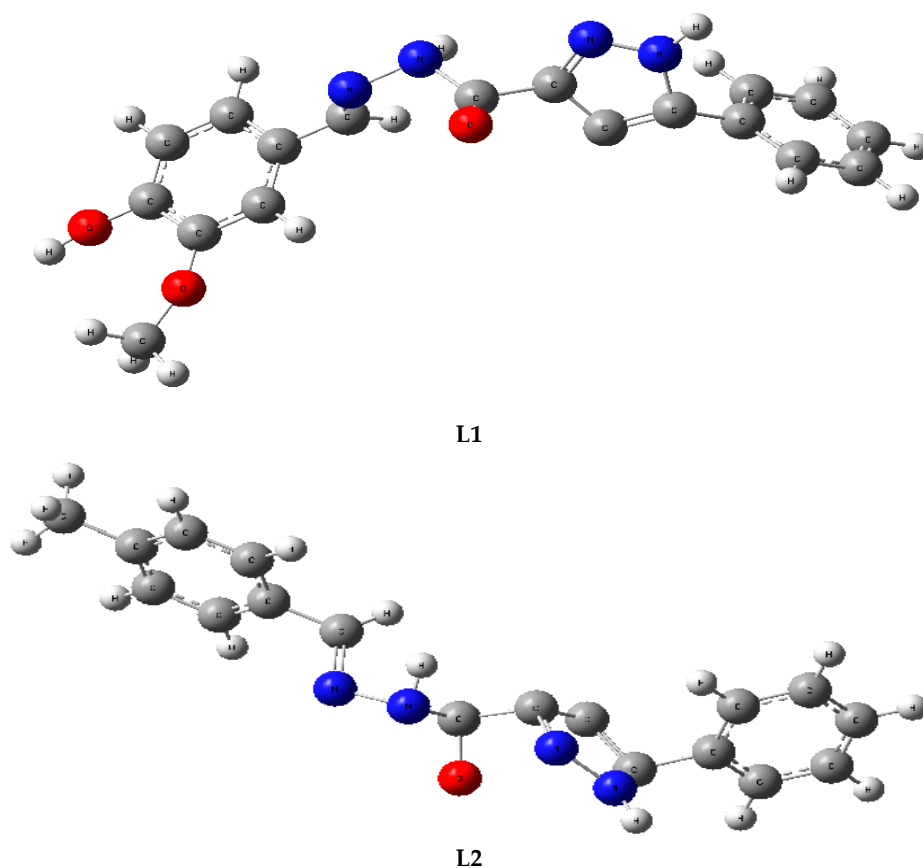


Figure 3. Optimized geometry of L1 and L2.

Table 2. Selected structural parameters by X-ray and theoretical calculations of compound L2.

Bond Length (Å)	Experimental Bond Lengths	Calculated Bond Lengths	Bond Angle (°)	Experimental Bond Angles	Calculated Bond Angles
O1–C10	1.22(2)	1.21	N2–N1–C7	113.4(15)	113.6
N1–N2	1.34(2)	1.34	N1–N2–C9	103.9(15)	105.4
N1–C7	1.34(3)	1.37	N4–N3–C10	119.2(17)	117.2
N2–C9	1.33(2)	1.34	N3–N4–C11	115.6(18)	114.2
N3–N4	1.38(2)	1.41	N1–C7–C6	122.7(17)	122.39
N3–C10	1.33(3)	1.36	N1–C7–C8	105.3(18)	103.59
N4–C11	1.26(3)	1.27	N2–C9–C8	111.4(16)	109.21
C15–C18	1.512(4)	1.50	N2–C9–C10	119.4(17)	119.83
N1–H	0.86(2)	1.00	N3–C10–C9	114.9(16)	111.05

The total energy, energy of HOMO and energy of LUMO, as well as other parameters for structures L1 and L2 are obtained theoretically and listed in Table 3. The HOMO and LUMO electron density distributions of L1 and L2 are given in Figures 4 and 5, respectively. After the analysis of the theoretical results obtained, we can say that molecules L1 and L2 have a non-planar structure. DFT calculation gives an idea about the substance reactivity and site selectivity of the frameworks. EHOMO; ELUMO, which clarifies the inevitable charge exchange collaboration inside the studied material; electronegativity (χ); hardness (η); potential (μ); electrophilicity (ω); softness (S); and softness (σ) are recorded in Table 3. The significance of η and σ is to evaluate both the reactivity and stability.

Table 3. Calculated energies of L1 and L2.

Molecular Energy (a.u.) (eV)	L1	L2
TE	-31008.6	-26911.4
E_{HOMO}	-5.8186	-6.4850
E_{LUMO}	-1.0152	-0.7349
Gap ΔE	4.8034	5.7500
Chemical potential μ (D)	5.8871	6.3122
Ionization potential (IP)	5.8186	6.4850
Electron affinity (EA)	1.0152	0.7349
Electron negativity (χ)	3.4169	3.6100
Global hardness (η)	2.4017	2.875
Global electrophilicity (ω)	2.4306	2.2664

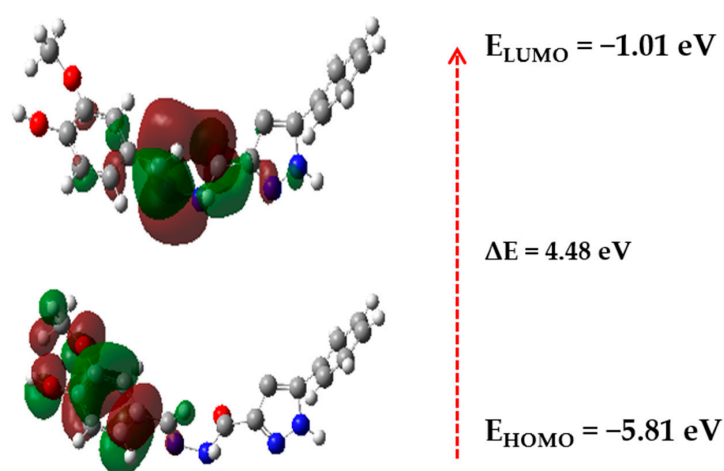


Figure 4. HOMO–LUMO energy diagram of L1.

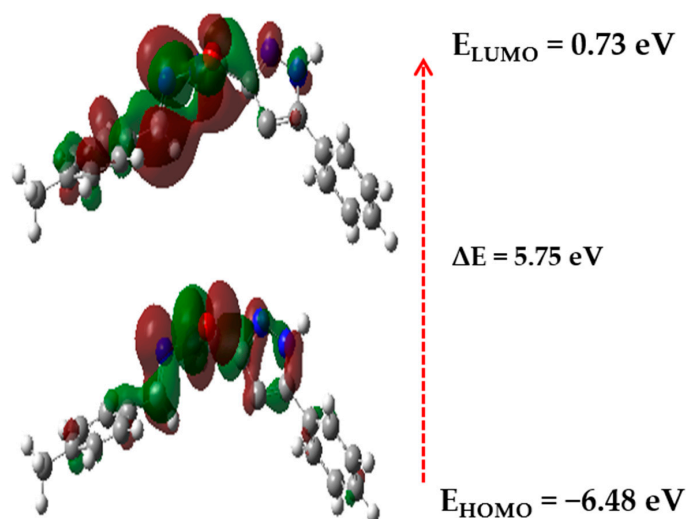


Figure 5. HOMO–LUMO energy diagram of L2.

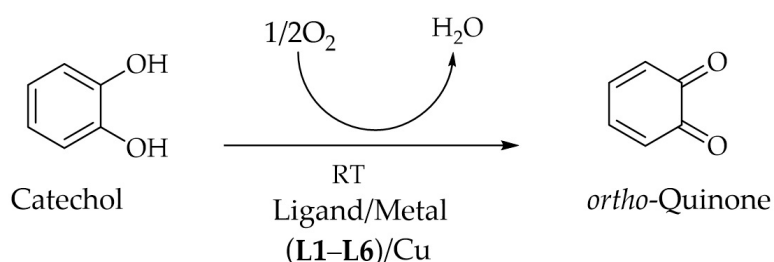
The analysis of the wave function indicates that the energy space between the molecular orbital HOMO and LUMO determines the chemical stability and the electrical transport properties of the molecule. The red and green colors of the molecular orbital ridge, respectively, represent the positive and negative phases.

The HOMO of **L1** shows the charge density localized on the 4-hydroxy-3-methoxybenzaldehyde ring, while LUMO is characterized by a charge distribution on the hydrazone function, indicating that this moiety can influence the electron transition. The HOMO of **L2** has a localized charge density on the pyrazole and hydrazone function, but LUMO is characterized by a charge distribution on the 4-methylbenzaldehyde ring and the hydrazone function. The energy difference between HOMO and LUMO of **L1** and **L2** is about 4.38 and 5.75 eV, respectively.

The energy of the smaller band space increases the stability of the molecule. The molecular boundary orbitals of **L1** and **L2** (HOMO–LUMO) are shown in Figures 4 and 5, respectively.

2.4. Catecholase Activity: Spectrophotometric Study

Catechol oxidation reaction catalyzed by copper complexes with ligands **L1–L6** is followed by the evolution of *o*-quinone absorbance measured at 390 nm with a UV-vis spectrometer (Scheme 2).



Scheme 2. Catecholase reaction.

The catalytic oxidation rate variations from one complex to another are shown in Figures S1–S5. On the other hand, catechol oxidation rates were calculated and collected in Table 4. According to these results, we find that all copper complexes, formed in situ from ligands **L1–L6** and salts of copper, catalyze the oxidation reaction of catechol to *o*-quinone, but with different rates. The catalytic activities depend highly on the ligand concentration, the nature of solvent and the type of inorganic anion (Figures S1–S5).

Table 4. Oxidation rate of catechol oxidation in methanol ($\mu\text{mol}\cdot\text{L}^{-1}\cdot\text{min}^{-1}$).

Ligand/Metallic Salt	Cu(NO ₃) ₂	CuCl ₂	Cu(CH ₃ COO) ₂	CuSO ₄
L1	10.57	10.28	9.80	9.27
L2	15.52	0.05	22.92	16.06
L3	37.89	9.19	24.58	21.01
L4	17.71	11.43	15.02	6.57
L5	3.10	8.07	19.62	10.61
L6	27.77	40.27	60.50	72.92

It appears plainly that catalytic activity varies from one complex to another. All of the copper complexes formed by the hydrazone derivatives catalyze the oxidation reaction of catechol to *o*-quinone. The best is the **L6** ligand with highest oxidation rate for all copper salts with maximum reaction rate equal to $72.92 \mu\text{mol}\cdot\text{L}^{-1}\cdot\text{min}^{-1}$ for CuSO₄ followed by **L3** with maximum rate of $37.89 \mu\text{mol}\cdot\text{L}^{-1}\cdot\text{min}^{-1}$ for Cu(NO₃)₂. Lowest recorded oxidation rates, whose values are less than $10 \mu\text{mol}\cdot\text{L}^{-1}\cdot\text{min}^{-1}$, correspond to complex **L2**-CuCl₂, followed by **L5**-(CuNO₃)₂ and **L4**-CuSO₄, and then **L5**-CuCl₂. The **L1** ligand seems to have nearly the same activity for all copper salts determined at about $10 \mu\text{mol}\cdot\text{L}^{-1}\cdot\text{min}^{-1}$.

Basically, for any ligand used except **L6**, Cu(CH₃COO)₂ gives highest activities and CuCl₂ gives lowest activities (Figure 6). Concerning CH₃COO[−] and ligands **L3**, **L4** and **L6**, the values of absorbance increase at the beginning of the reaction and then remain constant after a certain time. This has been

explained in previous studies by a precipitation of the complex that can take place during this decrease in absorbance.

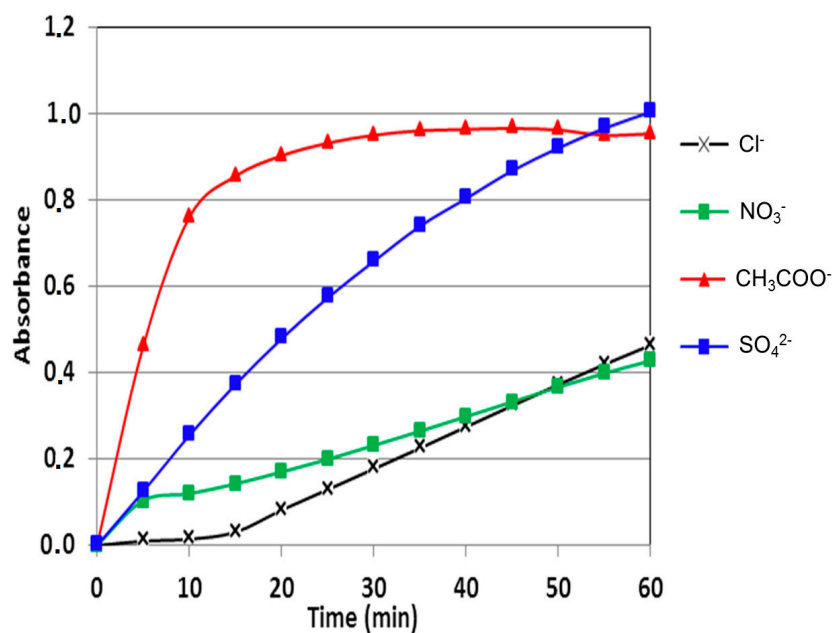


Figure 6. Catechol oxidation in the presence of copper complexes formed with L6.

2.4.1. Effect of Ligand Concentration on the Catecholase Activity

The effect of ligand concentration on catecholase activity is studied by varying the ratio of equivalent ligand L6: metallic salt $\text{Cu}(\text{CH}_3\text{COO})_2$. Three tests were carried out in ratios: 1:1, 2:1 and 1:2. The results obtained show that the test with the ratio L6: $\text{Cu}(\text{CH}_3\text{COO})_2 = 1:2$ leads to higher oxidation rate value. Therefore, the L6 complex that contains two cupric ion Cu(II) has a better catalytic activity. However, ratios 2:1 and 1:1 lead to lower oxidation rate value, and ratio 2:1 exhibits maximum at 35 min, and after slightly decreases, probably due to complex precipitation (Figure 7).

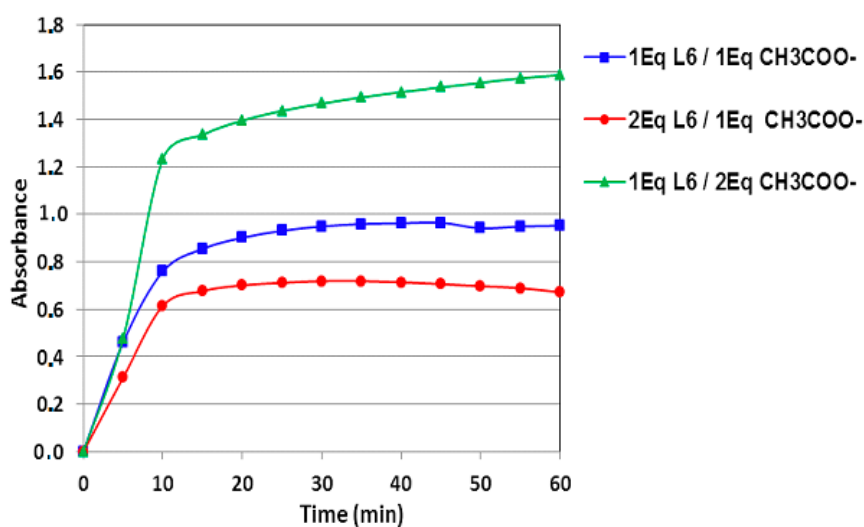


Figure 7. Catechol oxidation in methanol, in presence of formed L6 copper complexes with different concentrations.

2.4.2. Solvent Effect

The effect of three solvents (MeOH, CH₃CN and DMF) on the oxidation reaction with the ligand **L6** and the Cu(CH₃COO)₂ salt is studied in similar thermodynamic conditions. The results of that study are presented by the rate values obtained for the oxidation reaction (Figure 8). Using a polar protic solvent such as methanol promotes oxidation reaction much better than the other two aprotic solvents, i.e., acetonitrile and DMF. Our results seem to be in perfect agreement with previous studies and show that solvation of copper by the aprotic and polar solvents such as DMF and CH₃CN decreases the catalytic activity of the metal cation in the oxidation reaction of catechol to *o*-quinone.

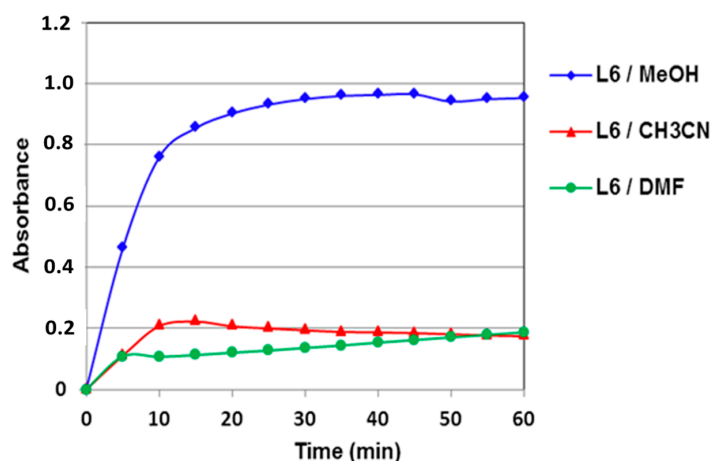


Figure 8. Catechol oxidation in different solvents and in the presence of formed **L6** copper complexes (1 Equivalent of **L6** for 1 Equivalent of Cu(CH₃COOH)₂).

2.4.3. Comparison with Alternative Catalysts

Table 5 shows the catalytic activity by other catalysts reported in the literature. It is clear that the hydrazone–pyrazole derivatives, in particular ligand **L6**, described in this work present further improvement and show better values and higher activity for the effective aerobic oxidation of the catechol into *o*-quinone.

Table 5. Comparison of the catalytic activity of various catalysts toward oxidation of the catechol into *o*-quinone, established in the same conditions, as given in previous literature.

Cu(II)-Ligands	Cu(II) Salt Used	Oxidation Rate ($\mu\text{mol}\cdot\text{L}^{-1}\cdot\text{min}^{-1}$)	Ref.
ligand L6	CuSO ₄	72.920	-
ligand L6	Cu(CH ₃ COO) ₂	60.500	-
ligand L6	CuCl ₂	40.270	-
<i>C,N</i> -bipyrazole bipyrazolic	Cu(CH ₃ COO) ₂	4.440	[29]
tripode-prop-2-ylacetate bipyrazolic	Cu(CH ₃ COO) ₂	11.825	[30]
tripode-4-hydroxyphenyl bipyrazolic	CuCl ₂	1.458	[31]
tripode-3-hydroxypropyl bipyrazolic	CuSO ₄	28.990	[32]
tripode-3-hydroxypropyl indole-3-chalcone	CuCl ₂	4.378	[33]
[(3,5-dimethyl-pyrazol-1-ylmethyl)-amino] -propionitrile	Cu(CH ₃ COO) ₂	31.780	[34]
	CuSO ₄	8.710	[35]

The superior catalytic activity observed for ligand **L6** is probably due to the stability of corresponding copper complex (catalyst) favored by the organic conjugate π bonds of the three benzene ring contained in the ligand and by the intense coordination bonds of the Schiff base. To our knowledge, the catalytic activity observed for ligand **L6** ($72.920 \mu\text{mol}\cdot\text{L}^{-1}\cdot\text{min}^{-1}$) is the most important among the catalysts described in the literature.

3. Experimental

3.1. General Methods

The chemical reagents used in synthesis were purchased from Merck, Darmstadt, Germany or Aldrich, St. Louis, MO, USA; were of the highest commercially available purity; and were used without previous purification. Melting points were measured using a Büchi B-545 digital capillary melting point apparatus (BUCHI Labortechnik AG, Flawil, CH, Switzerland) and used without correction. Reactions were checked with TLC silica gel 60 F254 (MACHEREY-NAGEL, Neumann-Neander, Drun, Germany). Spectra IR were recorded on a VERTEX 70 FT-IR spectrometer (Perkin-Elmer, Billerica, MA, USA) and frequencies are reported in cm^{-1} . The spectra of ^1H NMR and ^{13}C NMR were recorded in solution in $\text{DMSO}-d_6$ on a Bruker Avance 300 NMR spectrometer (Bruker, MA, USA). The chemical shifts are expressed in parts per million (ppm) by using tetramethylsilane (TMS) as internal reference and coupling constants (J) are given in Hz. Mass spectra were collected using a API 3200 LC/MS/MS system (AB MDS Sciex, Ontario, Canada) equipped with an ESI source. DRX data were collected on a Bruker APEX-II D8 Venture area diffractometer (Bruker, MA, USA) equipped with graphite monochromatic $\text{Mo K}\alpha$ radiation, $\lambda = 0.71073 \text{ \AA}$ at 293 (2) and 296 (2) K, respectively. The electronic spectra of the ligand and its metal complexes were measured on a Lambda 35 ES UV/VIS spectrophotometer (Perkin Elmer, Waltham, MA, USA) in the range of 200–900 nm.

3.2. Synthesis

3.2.1. Synthesis of 3-phenyl-1H-pyrazole-4-carbohydrazides (**2**)

To a stirred solution of 1 mmol of the 3-phenyl-1H-pyrazole-4-carboxylate (**1**) in ethanol (10 mL), 2 mL of 80% hydrazine monohydrate was added. The reaction mixture was maintained under reflux for 5 h, until TLC indicated the end of reaction. Afterwards, the reaction mixture was poured onto ice and the solid formed was collected by filtration, washed with cold water and recrystallized from ethanol. Yield: 66%; m.p: 207–209 °C; IR ($\nu(\text{cm}^{-1})$): 3296–3203 (NH, NH_2), 1629 (C=O); ^1H NMR: (300 MHz, $\text{DMSO}-d_6$, $\delta(\text{ppm})$): 4.45 (s, 2H, NH_2), 7.05 (1H, s, CH-pyrazole), 7.17–7.60 (5H, m, Ar-H), 9.38 (s, 1H, NHCO), 13.61 (1H, s, NH-pyrazole); ESI-MS: $m/z = 203.3$ [M+H] $^+$, 225.1 [M+Na] $^+$. The FT-IR, ^1H NMR and mass spectra of compound **2** are shown in Figures S6–S8.

3.2.2. General Procedure for the Synthesis of Ligands (**L1–L6**)

To a solution of 5-phenyl-1H-pyrazole-4-carbohydrazide (**2**) (1 mmol) in 10 mL of ethanol, an equimolar amount of the appropriate benzaldehyde derivative was added in the presence of acetic acid. The mixture was maintained under reflux for 2–5 h, until TLC indicated the end of reaction. Then, the reaction mixture was cooled to 25 °C, and the precipitate formed was filtered out washed with ethanol and recrystallized from ethanol. The FT-IR, (^1H , ^{13}C) NMR and mass spectra of Ligands (**L1–L6**) are shown in Figures S9–S30.

3.2.3. *N'*-(4-hydroxy-3-methoxybenzylidene)-5-phenyl-1H-pyrazole-3-carbohydrazide (**L1**)

Yield: 85%; m.p: 229–231 °C; IR ($\nu(\text{cm}^{-1})$): 3276 (NH), 1681 (C=O), 1568 (C=N); ^1H NMR: (300 MHz, $\text{DMSO}-d_6$, $\delta(\text{ppm})$): 3.81 (3H, s, $-\text{OCH}_3$), 6.83 (d, $J = 8.1$ Hz, 1H, H-Ar), 7.18 (1H, s, CH-pyrazole), 7.26–7.49 (5H, m, Ar-H), 7.54 (s, 1H, H-Ar), 7.82 (d, $J = 8.1$ Hz, 1H, H-Ar), 8.39 (1H, s, N=CH), 11.51 (s, 1H, OH), 11.72 (s, 1H, NHCO), 13.72 (1H, s, NH-pyrazole); ^{13}C NMR: (300 MHz,

DMSO- d_6 , δ (ppm)): 56.04 (OCH₃), 103.85 (CH, C4-pyrazole), 115.91 (CH, C-Ar), 122.53 (CH, C-Ar), 125.53 (CH, C-Ar), 126.37 (CH, C-Ar), 128.28 (CH, C-Ar), 129.07 (CHC-Ar), 129.33 (C, C-Ar), 129.54 (C-Ar), 144.12 (CH, N=CH), 145.85 (C, C3-pyrazole), 147.36 (C, C5-pyrazole), 148.63 (C, C-OH), 156.48 (C, C-OCH₃), 158.40 (C, C=O). ESI-MS: m/z = 337.0 [M+H]⁺, 359.0 [M+Na]⁺.

3.2.4. *N'*-(4-methylbenzylidene)-5-phenyl-1*H*-pyrazole-3-carbohydrazide (L2)

Yield: 90%; m.p: 297–299 °C; IR ($\nu(\text{cm}^{-1})$): 3205 (NH), 1680 (C=O), 1561 (C=N); ¹H NMR: (300 MHz, DMSO- d_6 , δ (ppm)): 2.32 (3H, s, CH₃), 7.25 (1H, s, CH-pyrazole), 7.33–7.61 (5H, m, Ar-H), 7.59 (d, J = 7.8 Hz, 2H, H-Ar), 7.81 (d, J = 7.8 Hz, 1H, H-Ar), 8.45 (1H, s, N=CH), 11.65 (s, 1H, NHCO), 13.78 (1H, s, NH-pyrazole); ¹³C NMR: (300 MHz, DMSO- d_6 , δ (ppm)): 21.50 (OCH₃), 103.85 (CH, C4-pyrazole), 125.80 (CH, C-Ar), 127.53 (CH, C-Ar), 127.90 (CH, C-Ar), 128.94 (CH, C-Ar), 129.49 (CH, C-Ar), 129.92 (C, C-Ar), 132.18 (C, C-Ar), 136.80 (C, C-CH₃), 140.28 (C, C3-pyrazole), 146.18 (CH, N=CH), 148.28 (C, C5-pyrazole), 158.50 (C, C=O). ESI-MS: m/z = 304.9 [M+H]⁺, 326.9 [M+Na]⁺.

3.2.5. *N'*-(4-chlorobenzylidene)-5-phenyl-1*H*-pyrazole-3-carbohydrazide (L3)

Yield: 89%; m.p: 301–303 °C; IR ($\nu(\text{cm}^{-1})$): 3207 (NH), 1680 (C=O), 1605 (C=N); ¹H NMR: (300 MHz, DMSO- d_6 , δ (ppm)): 7.11 (1H, s, CH-pyrazole), 7.33–7.60 (5H, m, Ar-H), 7.59 (d, J = 7.2 Hz, 2H, H-Ar), 7.81 (d, J = 7.2 Hz, 1H, H-Ar), 8.46 (1H, s, N=CH), 11.65 (s, 1H, NHCO), 13.79 (1H, s, NH-pyrazole); ¹³C NMR: (300 MHz, DMSO- d_6 , δ (ppm)): 103.82 (CH, C4-pyrazole), 125.82 (CH, C-Ar), 127.53 (CH, C-Ar), 127.90 (CH, C-Ar), 128.99 (CH, C-Ar), 129.49 (CH, C-Ar), 129.91 (C, C-Ar), 132.18 (C, C-Ar), 140.28 (C, C-CH₃), 148.20 (C, C3-pyrazole), 156.88 (CH, N=CH), 158.62 (C, C5-pyrazole), 164.13 (C, C=O). ESI-MS: m/z = 325.1 [M+H]⁺, 347.3 [M+Na]⁺.

3.2.6. *N'*-(4-fluorobenzylidene)-5-phenyl-1*H*-pyrazole-3-carbohydrazide (L4)

Yield: 98%; m.p: 294–296 °C; IR ($\nu(\text{cm}^{-1})$) : 3320 (NH), 1672 (C=O), 1604 (C=N); ¹H NMR: (300 MHz, DMSO- d_6 , δ (ppm)): 7.21 (1H, s, CH-pyrazole), 7.25–7.38 (5H, m, Ar-H), 7.42 (d, J = 7.8 Hz, 2H, H-Ar), 7.81 (d, J = 7.8 Hz, 1H, H-Ar), 8.50 (1H, s, N=CH), 11.72 (s, 1H, NHCO), 13.79 (1H, s, NH-pyrazole); ¹³C NMR: (300 MHz, DMSO- d_6 , δ (ppm)): 103.86 (CH, C4-pyrazole), 125.82 (CH, CH-Ar), 128.98 (CH, C-Ar), 129.49 (CH, CH-Ar), 129.64 (C, C-Ar), 129.74 (CH, CH-Ar), 130.10 (C, CH-Ar), 130.22 (C, C-Ar), 146.97 (C, C3-pyrazole), 150.50 (CH, N=CH), 156.68 (C, C5-pyrazole), 161.90 (C, C=O), 165.18 (C, C-F). ESI-MS: m/z = 309.3 [M+H]⁺.

3.2.7. 5-phenyl-*N'*-(1-phenylethylidene)-1*H*-pyrazole-3-carbohydrazide (L5)

Yield: 85%; m.p: 251–253 °C; IR ($\nu(\text{cm}^{-1})$) : 3320 (NH), 1667 (C=O), 1589 (C=N); ¹H NMR: (300 MHz, DMSO- d_6 , δ (ppm)): 2.36 (3H, s, CH₃), 7.24 (1H, s, CH-pyrazole), 7.42–7.84 (10H, m, Ar-H), 10.37 (s, 1H, NHCO), 13.82 (1H, s, NH-pyrazole); ¹³C NMR: (300 MHz, DMSO- d_6 , δ (ppm)): 21.51 (OCH₃), 103.60 (CH, C4-pyrazole), 125.73 (CH, C-Ar), 127.72 (CH, C-Ar), 128.70 (CH, C-Ar), 129.01 (CH, C-Ar), 129.18 (CH, C-Ar), 129.56 (CH, C-Ar), 130.34 (C, C-Ar), 132.07 (C, C-Ar), 137.21 (C, C3-pyrazole), 144.82 (CH, N=CH), 146.45 (C, C5-pyrazole), 157.23 (C, C=O). ESI-MS: m/z = 305.4 [M+H]⁺.

3.2.8. *N'*-(diphenylmethylene)-5-phenyl-1*H*-pyrazole-3-carbohydrazide (L6)

Yield: 82%; m.p: 200–202 °C; IR ($\nu(\text{cm}^{-1})$): 3360 (NH), 1664 (C=O), 1537 (C=N); ¹H NMR: (300 MHz, DMSO- d_6 , δ (ppm)): 7.20 (1H, s, CH-pyrazole), 7.32–7.76 (15H, m, Ar-H), 9.89 (s, 1H, NHCO), 13.84 (1H, s, NH-pyrazole); ¹³C NMR: (300 MHz, DMSO- d_6 , δ (ppm)): 105.10 (CH, C4-pyrazole), 127.66 (CH, C-Ar), 128.66 (CH, C-Ar), 128.96 (CH, C-Ar), 130.21 (CH, C-Ar), 130.31 (CH, C-Ar), 130.46 (CH, C-Ar), 132.02 (C, C-Ar), 137.28 (C, C-Ar), 141.08 (C, C3-pyrazole), 145.70 (CH, N=CH), 153.35 (C, C5-pyrazole), 157.62 (C, C=O). ESI-MS: m/z = 366.9 [M+H]⁺, 389.0 [M+H]⁺.

3.3. X-Ray Crystallographic Analysis

The compounds of **L1** and **L2** were obtained as single crystals by slow evaporation from ethanol solution of the pure compound at room temperature. Cell refinement and data reduction were carried out by Bruker SAINT. SHELXT was used to solve structure [36,37]. The final refinement was carried out by full-matrix least-squares techniques with anisotropic thermal data for no hydrogen atoms on *F*. CCDC 1522882 and 1523265 for **L1** and **L2**, respectively, contain the supplementary crystallographic data for these compounds can be obtained free of charge from the Cambridge Crystallographic Data Centre via http://www.ccdc.cam.ac.uk/data_request/cif.

3.4. DFT Computational Method

The computational studies of compounds **L1** and **L2** were performed at the B3LYP/6-31G level of theory using Gaussian 09 package programs [38,39]. The optimization geometries of **L1** and **L2** were performed using the Bery analytical gradient optimization method [40].

3.5. Catecholase Activity Measurement

Kinetic measurements were made spectrophotometrically on UV-vis spectrometer, following the appearance of *o*-quinone over time at 25 °C (390 nm absorbance maximum $\epsilon = 1600 \text{ L mol}^{-1} \text{ cm}^{-1}$ in methanol [35]). The complexes were prepared in situ by successively mixing 0.15 mL of a solution ($2 \times 10^{-3} \text{ M}$) of $\text{CuX}_2 \cdot n\text{H}_2\text{O}$ ($X = \text{Cl}^-$, NO_3^- , CH_3COO^- or SO_4^{2-}), with 0.15 mL of a solution ($2 \times 10^{-3} \text{ M}$) of ligand, then adding 2 mL of a solution of catechol at a concentration of 10^{-1} M .

4. Conclusions

In this work, we report the synthesis of six new hydrazone–pyrazole biomolecules (**L1–L6**) in excellent yields. The X-ray structures of **L1** and **L2** have been investigated herein for the first time. The theoretical calculations through DFT of **L1** and **L2** well supported the experimental findings. These ligands (**L1–L6**) and different Cu(II) salts demonstrate an efficient activity to catalyze the aerobic oxidation of the catechol into *o*-quinone compared to others recent catalysts described in the literatures. Interestingly, ligand **L6** exhibits an extremely high rate of oxidation, attaining $72.92 \mu\text{mol} \cdot \text{L}^{-1} \cdot \text{min}^{-1}$, which is, to our knowledge, the best catalytic activity among the reported catalysts. Cu(II)-ligand complexes were generated in situ and the results obtained show that the oxidation depend highly on several parameters: the nature and concentration of the ligand, the nature of salts and the solvent effects. The results suggest that these new materials have potential for the oxidation of the catechol into *o*-quinone, thus opening important perspectives.

Supplementary Materials: Supplementary materials can be found at www.mdpi.com/1422-0067/18/11/2215/s1.

Acknowledgments: The authors extend their appreciation to the PPR2-MESRSFC-CNRST-P10 project (Morocco) for supporting this work. Sincere appreciation is also extended to the Deanship of Scientific Research at King Saud University for supporting this Prolific Research group (PRG-1437-29).

Author Contributions: Khalid Karrouchi, Smaail Radi and M'hammed Ansar carried out of the experimental work and cooperated in the preparation of the manuscript. Nada Kheira Sebbar and Younes Ouzidan performed the density functional theory calculations. Yahia N. Mabkhot and Hazem A. Ghabbour determined the X-ray crystal structure and Yahia N. Mabkhot also paid the publication fees. Youssef Ramli performed the structural analysis and description. El Bekkaye Yousfi carried out the catalytic activity. Jamal Taoufik cooperated in the preparation of the manuscript, interpretation of the results.

Conflicts of Interest: The authors declare no conflict of interest.

References

1. Hartinger, C.G.; Dyson, P.J. Bioorganometallic chemistry—from teaching paradigms to medicinal applications. *Chem. Soc. Rev.* **2009**, *38*, 391–401. [[CrossRef](#)] [[PubMed](#)]
2. Patra, M.; Gasser, G. Organometallic Compounds: An Opportunity for Chemical Biology? *ChemBioChem* **2012**, *13*, 1232–1252. [[CrossRef](#)] [[PubMed](#)]

3. Daumann, L.J.; Schenk, G.; Ollis, D.L.; Gahan, L.R. Spectroscopic and mechanistic studies of dinuclear metallohydrolases and their biomimetic complexes. *Dalton Trans.* **2014**, *43*, 910–928. [[CrossRef](#)] [[PubMed](#)]
4. Dalle, K.E.; Meyer, F. Modelling binuclear metallobiosites: Insights from pyrazole-supported biomimetic and bioinspired complexes. *Eur. J. Inorg. Chem.* **2015**, *2015*, 3391–3405. [[CrossRef](#)]
5. Mistri, S.; Paul, A.; Bhunia, A.; Manne, R.K.; Santra, M.K.; Puschmann, H.; Manna, S.C. A combined experimental and theoretical investigation on the Cu(II) sensing behavior of a piperazinyl moiety based ligand, and catecholase and biological activities of its Cu(II) complex in combination with pyridine 2,5-dicarboxylate. *Polyhedron* **2016**, *104*, 63–72. [[CrossRef](#)]
6. Rosenzweig, A.C.; Sazinsky, M.H. Structural insights into dioxygen-activating copper enzymes. *Curr. Opin. Struct. Biol.* **2006**, *16*, 729–735. [[CrossRef](#)] [[PubMed](#)]
7. Mirica, L.M.; Ottenwaelder, X.; Stack, T.D.P. Structure and Spectroscopy of Copper–Dioxygen Complexes. *Chem. Rev.* **2004**, *104*, 1013–1046. [[CrossRef](#)] [[PubMed](#)]
8. Itoh, S.; Fukuzumi, S. Monooxygenase Activity of Type 3 Copper Proteins. *Acc. Chem. Res.* **2007**, *40*, 592–600. [[CrossRef](#)] [[PubMed](#)]
9. Mutti, F.G.; Zoppellaro, G.; Gullotti, M.; Santagostini, L.; Pagliarin, R.; Andersson, K.K.; Casella, L. Biomimetic Modelling of Copper Enzymes: Synthesis, Characterization, EPR Analysis and Enantioselective Catalytic Oxidations by a New Chiral Trinuclear Copper(II) Complex. *Eur. J. Inorg. Chem.* **2009**, *2009*, 554–566. [[CrossRef](#)]
10. Balasubramanian, V.; Ezhevskaya, M.; Moons, H.; Neuburger, M.; Cristescu, C.; Van Doorslaer, S.; Palivan, C. Structural characterization of a highly active superoxide-dismutase mimic. *Phys. Chem. Chem. Phys.* **2009**, *11*, 6778–6787. [[CrossRef](#)] [[PubMed](#)]
11. Sreenivasulu, B. Diphenoxo-Bridged Copper(II) Complexes of Reduced Schiff Base Ligands as Functional Models for Catechol Oxidase. *Aust. J. Chem.* **2009**, *62*, 968–979. [[CrossRef](#)]
12. Solomon, E.I.; Sundaram, U.M.; Machonkin, T.E. Multicopper Oxidases and Oxygenases. *Chem. Rev.* **1996**, *96*, 2563–2606. [[CrossRef](#)] [[PubMed](#)]
13. Eicken, C.; Krebs, B.; Sacchettini, J.C. Catechol oxidase—structure and activity. *Curr. Opin. Struct. Biol.* **1999**, *9*, 677–683. [[CrossRef](#)]
14. Beyazit, N.; Çatıkkaş, B.; Bayraktar, Ş.; Demetgül, C.J. Synthesis, characterization and catecholase-like activity of new Schiff base metal complexes derived from visnagin: Theoretical and experimental study. *J. Mol. Struct.* **2016**, *1119*, 124–132. [[CrossRef](#)]
15. Shaban, S.Y.; Ramadan, A.E.-M.M.; Ibrahim, M.M.; Mohamed, M.A.; van Eldik, R. Spectroscopic, thermodynamic, kinetic studies and oxidase/antioxidant biomimetic catalytic activities of tris(3,5-dimethylpyrazolyl)borate Cu(II) complexes. *Dalton Trans.* **2015**, *44*, 14110–14121. [[CrossRef](#)] [[PubMed](#)]
16. Comba, P.; Martin, B.; Muruganatham, A.; Straub, J. Structure, Bonding, and Catecholase Mechanism of Copper Bispidine Complexes. *Inorg. Chem.* **2012**, *51*, 9214–9225. [[CrossRef](#)] [[PubMed](#)]
17. Ackermann, J.; Buchler, S.; Meyer, F. Structure–activity correlations in highly preorganized dicopper catechol oxidase model systems. *C. R. Chim.* **2007**, *10*, 421–432. [[CrossRef](#)]
18. Belle, C.; Selmeçzi, K.; Torelli, S.; Pierre, J.-L. Chemical tools for mechanistic studies related to catechol oxidase activity. *C. R. Chim.* **2007**, *10*, 271–283. [[CrossRef](#)]
19. Matoga, D.; Szklarzewicz, J.; Stadnicka, K.; Shongwe, M.S. Iron (III) complexes with a biologically relevant aroylhydrazone: crystallographic evidence for coordination versatility. *Inorg. Chem.* **2007**, *46*, 9042–9044. [[CrossRef](#)] [[PubMed](#)]
20. Shongwe, M.S.; Al-Rahbi, S.H.; Al-Azani, M.A.; Al-Muharbi, A.A.; Al-Mjeni, F.; Matoga, D.; Gismelseed, A.; Al-Omari, I.A.; Yousif, A.; Adams, H.; et al. Coordination versatility of tridentate pyridyl aroylhydrazones towards iron: tracking down the elusive aroylhydrazono-based ferric spin-crossover molecular materials. *Dalton Trans.* **2012**, *41*, 2500–2514. [[CrossRef](#)] [[PubMed](#)]
21. Anbu, S.; Paul, A.; Ribeiro, A.P.C.; da Silva, M.F.C.G.; Kuznetsov, M.L.; Pombeiro, A.J.L. Biomolecular interaction, catecholase like activity and alkane oxidation in ionic liquids of a phenylcarbohydrazone-based monocopper(II) complex. *Inorg. Chim. Acta* **2016**, *450*, 426–436. [[CrossRef](#)]
22. Ruben, M.; Lehn, J.-M.; Vaughan, G. Synthesis of ionisable [2 × 2] grid-type metallo-arrays and reversible protonic modulation of the optical properties of the [Co^{II}₄L₄]⁸⁺ species. *Chem. Commun.* **2003**, *12*, 1338–1339. [[CrossRef](#)]

23. Mondal, S.; Pakhira, B.; Blake, A.J.; Drew, M.G.B.; Chattopadhyay, S.K. Co(III) and Ni(II) complexes of an anthracene appended aroyl hydrazine: Synthesis, crystal structures, DNA binding and catecholase activity. *Polyhedron* **2016**, *117*, 327–337. [CrossRef]
24. Katyal, M.; Dutt, Y. Analytical applications of hydrazones. *Talanta* **1975**, *22*, 151–166. [CrossRef]
25. Mohan, M.; Gupta, M.P.; Chandra, L.; Jha, N.K. Synthesis, characterization and antitumour properties of some metal (II) complexes of 2-pyridinecarboxaldehyde 2'-pyridylhydrazone and related compounds. *Inorg. Chim. Acta* **1988**, *151*, 61–68. [CrossRef]
26. Karrouchi, K.; Charkaoui, Y.; Benlafya, K.; Ramli, Y.; Taoufik, J.; Radi, S.; Ansar, M. Synthesis, characterization and preliminary biological activity of some new pyrazole carbohydrazide derivatives. *J. Chem. Pharm. Res.* **2013**, *5*, 1–6.
27. Karrouchi, K.; Radi, S.; Taoufik, J.; Ghabbour, H.A.; Mabkhot, Y.N. Crystal structure of *N'*-(4-nitrobenzylidene)-5-phenyl-1*H*-pyrazole-3-carbohydrazide, C₁₇H₁₃N₅O₃. *Z. Krist. New Cryst. Struct.* **2016**, *231*, 839–841. [CrossRef]
28. Karrouchi, K.; Ansar, M.; Radi, S.; Saadi, M.; El Ammari, L. Crystal structure of *N'*-diphenylmethylidene-5-methyl-1*H*-pyrazole-3-carbohydrazide. *Acta Crystallogr. E Crystallogr. Commun.* **2015**, *71*, o890–o891. [CrossRef] [PubMed]
29. El Kodadi, M.; Malek, F.; Touzani, R.; Ramdani, A. Synthesis of new tripodal ligand 5-(bis(3,5-dimethyl-1*H*-pyrazol-1-ylmethyl)amino)pentan-1-ol, catecholase activities studies of three functional tripodal pyrazolyl *N*-donor ligands, with different copper (II) salts. *Catal. Commun.* **2008**, *9*, 966–969. [CrossRef]
30. Boussaleh, N.; Touzani, R.; Bouabdallah, I.; El Kadiri, S.; Ghalem, S. Synthesis, structure and catalytic properties of tripodal amino-acid derivatized pyrazole-based ligands. *J. Mol. Catal. A Chem.* **2009**, *306*, 113–117. [CrossRef]
31. Bouabdallah, I.; Touzani, R.; Zidane, I.; Ramdani, A. Synthesis of new tripodal ligand: *N,N*-bis[(1,5-dimethylpyrazol-3-yl)methyl]benzylamine.: Catecholase activity of two series of tripodal ligands with some copper (II) salts. *Catal. Commun.* **2007**, *8*, 707–712. [CrossRef]
32. Zerrouki, A.; Touzani, R.; El Kadiri, S. Synthesis of new derivatized pyrazole based ligands and their catecholase activity studies. *Arab. J. Chem.* **2011**, *4*, 459–464. [CrossRef]
33. Mouadili, A.; Attayibat, A.; El Kadiri, S.; Radi, S.; Touzani, R. Catecholase activity investigations using in situ copper complexes with pyrazole and pyridine based ligands. *Appl. Catal. A Gen.* **2013**, *454*, 93–99. [CrossRef]
34. Thabti, S.; Djedouani, A.; Rahmouni, S.; Touzani, R.; Bendaas, A.; Mousser, H.; Mousser, A. Synthesis, X-ray crystal structures and catecholase activity investigation of new chalcone ligands. *J. Mol. Struct.* **2015**, *1102*, 295–301. [CrossRef]
35. Mouadili, A.; Zerrouki, A.; Herrag, L.; Hammouti, B.; El Kadiri, S.; Touzani, R. Catechol oxidation: activity studies using electron-rich nitrogen-based ligands. *Res. Chem. Intermed.* **2012**, *38*, 2427–2433. [CrossRef]
36. Sheldrick, G.M. A short history of SHELX. *Acta Crystallogr.* **2008**, *64*, 112–122. [CrossRef] [PubMed]
37. Sheldrick, G.M. *Program SHELXTL97*; Siemens Analytical X-ray Instruments, Inc.: Madison, WI, USA, 1997.
38. Becke, A.D. Density-functional thermochemistry. III. The role of exact exchange. *Chem. Phys.* **1993**, *98*, 5648. [CrossRef]
39. Frisch, M.J.; Trucks, G.W.; Schlegel, H.B.; Scuseria, G.E.; Robb, M.A.; Cheeseman, J.R.; Scalmani, G.; Barone, V.; Mennucci, B.; Petersson, G.A.; et al. *Gaussian 09, Revision E.01*; Gaussian, Inc.: Wallingford CT, England, 2009.
40. Becke, A.D. Density-functional exchange-energy approximation with correct asymptotic behavior. *Phys. Rev.* **1988**, *38*, 3098. [CrossRef]

